Mechanical and Hydrothermal Stabilities of Aged Periodic Mesoporous Organosilicas

Mark C. Burleigh,† Michael A. Markowitz,* Shalini Jayasundera, Mark S. Spector, Chris W. Thomas, and Bruce P. Gaber

Laboratory for Molecular Interfacial Interactions, Code 6930, Center for Bio/Molecular Science and Engineering, Naval Research Laboratory, Washington, DC 20375

Received: May 2, 2003; In Final Form: August 20, 2003

Methylene-, ethylene-, and phenylene-bridged periodic mesoporous organosilicas (PMOs) synthesized with nonionic alkylethylene oxide templates exhibited significantly better mechanical and hydrothermal stabilities than periodic mesoporous silica. Synthesis of PMOs utilized the acid-catalyzed hydrolysis and condensation of bis(triethoxysilyl) precursors around supramolecular polyoxyethylene(10) stearyl ether (Brij 76) templates. Nitrogen gas sorption, thermogravimetry, and X-ray diffraction have been used to characterize the effects of aging, mechanical compression, and hydrothermal treatment on these materials. Both as-synthesized composites containing surfactant templates and extracted PMOs showed no degradation after 10 months. The enhanced stability of these nanoporous organosilicas relative to meoporous silica makes them potential candidates for use in advanced catalysis and adsorption applications.

Introduction

The discovery of the M41S family of mesoporous molecular sieves[1,2] has led to great scientific interest in the field of porous materials. One member of this family, MCM-41, with its hexagonal arrays of uniform pore channels has been of particular interest because of its potential for catalytic and adsorbent applications. The ordered microstructure and relatively large pore size of MCM-41 allows for fast diffusion of molecules leading to quick access to its large internal surface areas. The surfactant template approach used to synthesize these materials allows one to control the pore size (∼2−10 nm) by the appropriate choice of surfactant and synthetic conditions.[3,4] Pore size control gives one the ability to design catalysts and adsorbents that allow or deny access to specific molecules to the reaction events that take place within the pores. This size selectivity is particularly advantageous in the mesoporous range because this allows for the "sieving" of moderately sized molecules, all of which are excluded from microporous zeolites.

Unfortunately, these materials lack the hydrothermal and mechanical stability commonly required for catalysis and adsorption. This could limit their potential industrial applications. Ryoo and Kim[5] reported that the ordered microstructures of hexagonal MCM-41 and cubic MCM-48 disintegrate readily in boiling water. Characterization by X-ray powder diffraction and ^{29}Si solid-state NMR indicates that the mechanism for this disintegration is silicate hydrolysis. It has since been shown that the hydrothermal stability can be improved in a number of ways. These include the addition of large concentrations of various salts during synthesis,[6,7] the synthesis of ordered microstructures with thicker pore walls,[8,9] and the substitution of silicon with aluminum.[10,11] Exposure to water, even under mild conditions, has been shown to degrade ordered mesoporous silica. Broyer et al. have reported a 54% decrease in the pore volume of freshly calcined MCM-41 after 3 months under ambient conditions.[12] When it was stored under dry nitrogen for the same time period, no significant change was noted. The microstructures of ordered mesoporous silicas have also been shown to undergo considerable damage upon mechanical compression.[9,13,14] This damage can be reduced significantly by the careful exclusion of moisture,[15] increasing the hydrophobicity of the silica surface by trimethylsilylation,[13] or increasing the pore wall thickness.[9]

Because of their vulnerability to silicate hydrolysis, the lack of structural integrity in mesoporous silicas can be overcome by eliminating water. Because evacuating materials and storing them under dry nitrogen can be expensive, tailoring the surfaces of ordered porous materials with nonpolar functional groups may be a more practical approach. The incorporation of organic functional groups into nanoporous materials has been accomplished by employing a number of different synthetic strategies.[16−21] The most effective method for functionalizing ordered nanoporous materials involves the use of bis(alkoxysilyl) precursors containing organic bridging groups. This method incorporates the organic functionality directly into the pore walls simply by the selection of the appropriate precursor[22] and was first reported by Inagaki and co-workers.[23] This synthetic approach eliminates the multistep protocols required in postsynthetic grafting techniques.[16−18] It also avoids the problems associated with different precursor hydrolysis rates and reduced order incurred during co-condensation polymerizations.[19−21] The hydrophobicity imparted on periodic mesoporous organosilicas (PMOs) due to the presence of organic bridging groups should increase their aging, hydrothermal, and mechanical stabilities. Stein and co-workers reported that an ethylene-bridged PMO synthesized with alkyltrimethylammonium templates in basic media had better hydrothermal stability than MCM-41.[24] We have recently reported the synthesis of a new family of PMOs using neutral alkylethylene oxide templates in acidic media.[25,26] These PMOs have large surface areas, ordered microstructures, and thick pore walls. The hydrophobic surface groups and thick pore walls may enhance the hydrothermal and mechanical stability of these materials.

In this paper, we examine the effects of aging, mechanical, and hydrothermal treatments on the microstructure of our PMOs. Specifically, we have used nitrogen gas sorption, thermogravimetric analysis, and powder X-ray diffraction to characterize methylene, ethylene, and phenylene-bridged nanoporous orga-

† Deceased.

10.1021/jp035189q CCC: $25.00
Published on Web 10/29/2003

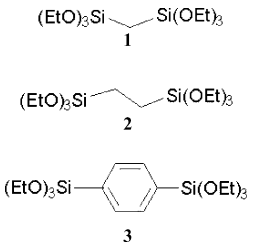

Figure 1. Structures of the PMO precursors: (1) bis(triethoxysilyl)-methylene; (2) bis(triethoxysilyl)ethylene; (3) 1,4-bis(triethoxysilyl)-benzene.

nosilicas before and after such treatments. Solid-state NMR was used to characterize the nanoporous materials before and after surfactant template extraction. The stabilities of these materials have been compared to that of nanoporous silica synthesized under similar conditions. The mechanical stabilities of the as-synthesized composite materials containing surfactant templates have also been compared to those of the surfactant template extracted nanoporous materials derived from them.

Materials and Methods

Chemicals. The PMO precursors used include bis(triethoxysilyl)methylene, bis(triethoxysilyl)ethylene, and 1,4-bis(triethoxysilyl)benzene (Figure 1). The synthesis of the 1,4-bis(triethoxysilyl)benzene monomer was carried out in house (see monomer synthesis), while the other organosilanes were obtained from Gelest, Inc. Ligroin (Fisher) was used without further purification. All other chemicals were obtained from Aldrich and used as received. Water used in all synthetic procedures was deionized to 18 MΩ cm.

Characterization. Solid-state cross-polarization magic angle spinning (CP MAS) ^{13}C NMR experiments were performed at room temperature on a Bruker DMX-500 MHz at a resonance frequency of 125.77 with a 4.0 mm MAS probe. The samples were packed in 4 mm zirconia Bruker rotors fitted with Kel-F end caps for magic angle spinning at 10−12.5 kHz. A two-pulse phase modulation (TPPM) decoupling was used for proton decoupling.[27] A ^{13}C CP contact time of 2 ms was used for all of the samples with up to 1000 scans and 10 s delays. The ^{13}C reference was set to external tetrakis(trimethylsilyl) silane at 3.5 ppm with respect to TMS at 0 ppm. X-ray diffraction measurements were made on an Enraf-Nonius FR591 rotating anode operating at 13 kW. A singly bent graphite monochromator selected Cu Kα radiation and provided in-plane resolution of 0.014 Å^{-1} full width at half-maximum. Powder samples were placed in 1.0 mm quartz capillary tubes. Gas sorption experiments were performed using a Micromeritics ASAP 2010. Nitrogen gas was used as the adsorbate at 77 K. Thermogravimetric analyses were performed with a TA Instruments TGA 2950 thermogravimetric analyzer. All measurements were made in high-resolution dynamic mode.

Monomer Synthesis: 1,4-Bis(triethoxysilyl)benzene. A N_2-purged three-neck round-bottom flask with stir bar and magnesium turnings (15 g, 0.62 mol) was flame-dried before adding TEOS (450 mL, 2 mol), dry THF (250 mL), and a few crystals of iodine. The solution was brought to reflux (65 °C) and *p*-dibromobenzene (48 g, 0.20 mol) in THF (125 mL) was added dropwise to the flask during 2 h. This solution was allowed to reflux during another 1.5 h, becoming dark yellow. After the solution cooled to room temperature, the THF was removed by rotary evaporation, and ca. 200 mL of ligroin was added to precipitate MgBr; it was removed by vacuum filtration. The liquor was condensed by rotary evaporation and subjected to vacuum distillation to remove excess TEOS (65 °C, 0.5 Torr), followed by product (130 °C, 0.2 Torr), which appeared as a colorless oil (30 g, recovered yield 37%). ^{1}H NMR (400 MHz, $CDCl_3$/TMS) δ 7.68 (s, 4H), 3.87 (quartet, 12H), 1.24 (t, 18H). ^{13}C NMR (100.7 MHz, $CDCl_3$/TMS) δ 134.0, 133.2, 58.7, 18.1.

PMO Synthesis. The method previously described for the synthesis of periodic nanoporous ethane silica[25] was modified by the use of a specific amount of HCl and the appropriate organosilane precursor (Figure 1). Concentrated HCl (13.1 mL, 12.2 M) was added to deionized water (186.9 mL) to make the initial aqueous solutions. The Brij 76 ($C_{18}H_{37}(OCH_2OCH_2)_{10}$-OH, 4.0 g) surfactant template was added to the 200 mL solutions upon stirring, and the mixtures were covered and heated at 50 °C for 12h. The precursors were then added to the resulting clear solutions. The reactant molar ratios were as follows: 0.11 Brij 56/222 H_2O/3.20 HCl/0.56 organosilane.

The synthesis mixtures were covered and stirred at 50 °C for 12 h, followed by heating at 90 °C under static conditions for an additional 24 h. The precipitates were recovered by suction filtration and air-dried. A portion of these as-synthesized nanoscopic composites were characterized, while the remaining amount was extracted with acidified ethanol to produce nanoporous organosilicas. A pure silica analogue was prepared by substituting an equimolar amount of tetramethyl orthosilicate (TMOS) for the bis(alkoxysilyl) precursors.

Postsynthetic Treatment. As-synthesized nanoscopic composites were placed in excess (350 mL/g) acidified ethanol (1 M HCl) and refluxed for 6 h to extract the surfactant template. The products were recovered by filtration, washed with absolute ethanol, and dried under vacuum at 60 °C for 10 h. The extraction procedure was repeated twice.

Aging. Following postsynthetic treatment, a portion of each nanoporous material was aged for 10 months under ambient conditions. These samples were simply placed in open vials on a shelf. No special attempts were made to control either the temperature or humidity.

Mechanical Treatment. The aged powders were placed in a 13 mm die and compressed for 30 min at various pressures. The samples were not placed in a vacuum oven prior to pressing, and no vacuum was applied to the die to remove any moisture adsorbed on their surfaces.

Hydrothermal Treatment. The aged nanoporous powders were boiled in deionized water for 18 h, isolated by suction filtration, and dried under vacuum at 60 °C for 10 h.

Results and Discussion

Aging Stability. Powder X-ray diffraction and nitrogen gas sorption analyses were performed on all of the extracted nanoporous materials before and after aging. Solid-state ^{13}C CP MAS NMR spectroscopy was used to show the successful removal of the surfactant templates during the postsynthetic extraction and the stable Si−C bonding throughout the synthesis. The ^{13}C CP MAS NMR spectra of the as-synthesized and extracted methylene (A), ethylene (B), phenylene (C), and silica (D) nanoporous materials are shown in Figure 2. All four sets of spectra show the disappearance of the primary surfactant resonances located at $\delta \approx 30$ and 70 ppm after extraction indicating near-complete removal of the surfactant using the acidified ethanol extraction method. The small resonances at $\delta \approx 18$ (methyl) and 58 (methylene) ppm in the extracted spectra are associated with trace amounts of ethanol used in the extraction process.

A comparison of the physicochemical properties of the nanoporous organosilicas (Table 1) shows little evidence of any

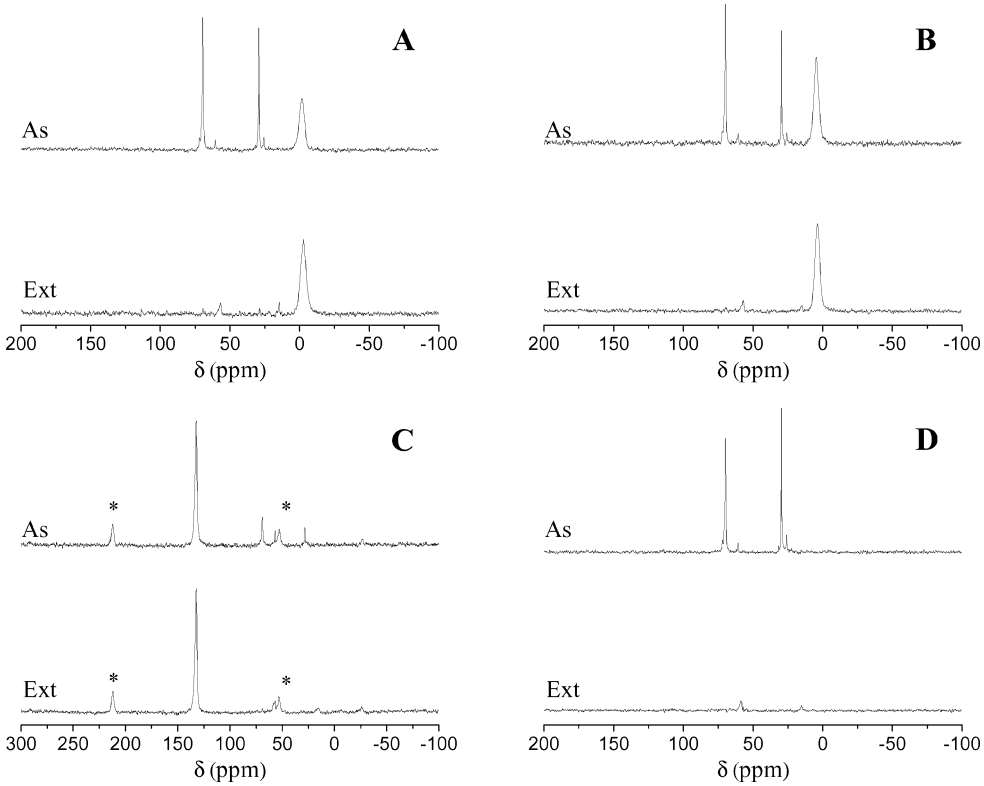

Figure 2. ^{13}C CP MAS NMR spectra of as-synthesized (As) and template surfactant extracted (Ext) (A) methylene, (B) ethylene, (C) phenylene, and (D) silica nanoporous materials.

TABLE 1: Structural Properties of Extracted Nanoporous Organosilicas before and after Aging

sample	D^a (Å)	BET surface area (m^2/g)	total pore volume (cm^3/g)	pore size^b (Å)	wall thickness^c (Å)
methylene PMO	74	880	0.90	50	35
methylene PMO (aged)	74	872	0.90	50	35
ethylene PMO	61	1070	1.10	44	26
ethylene PMO (aged)	63	1080	1.10	43	29
phenylene PMO	59	940	0.70	35	33
phenylene PMO (aged)	57	901	0.60	33	33
nanoporous silica	61	990	1.40	46	24
nanoporous silica (aged)	59	1010	1.30	44	24

[a] $d(100)$ spacing of the extracted products (±2 Å). [b] Calculated from adsorption branch. [c] Estimated from a_0-pore size, where $a_0 = (2\sqrt{3}/3)d(100)$.

microstructural changes as a result of the aging process. The phenylene-bridged PMO does exhibit slight decreases in the BET surface area (~4%) and total pore volume (~10%). The substantial decrease in total pore volume reported by Bellat and co-workers[12] for calcined MCM-41 materials after aging under ambient conditions is not exhibited by any of our nanoporous materials. The difference in the aging stability of these materials may be due to the rather large discrepancy in pore wall thickness. The MCM-41 materials synthesized with alkylammonium templates in basic media exhibited relatively thin (7−10 Å) pore walls. All of our nanoporous materials synthesized with alkylethylene oxide templates in acidic media exhibit much thicker (24−35 Å) walls.[26]

Mechanical Stability. The aged extracted nanoporous powders were first pressed at 8000 lb (268 MPa) for 30 min. The methylene- and phenylene-bridged PMOs and the nanoporous silica formed hard disks during compression and had to be ground with a mortar and pestle prior to nitrogen sorption and

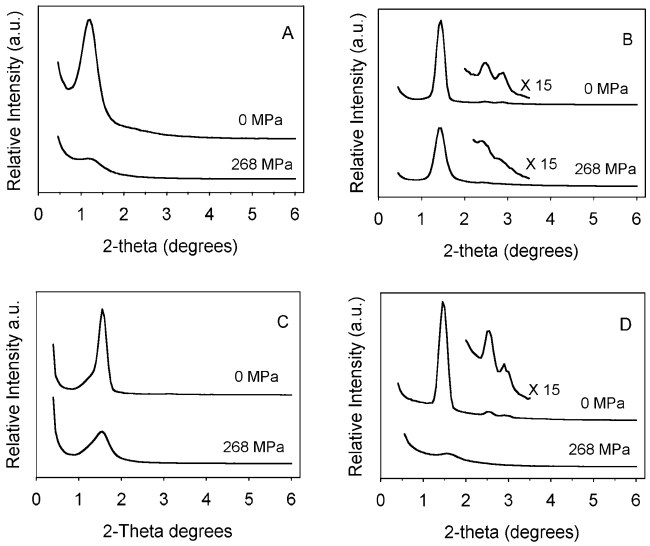

Figure 3. Powder X-ray diffraction patterns of the template-extracted (A) methylene, (B) ethylene, (C) phenylene, and (D) silica nanoporous materials before and after pressure treatment at 268 MPa for 30 min.

powder X-ray analyses. The ethylene-bridged PMO remained a fluffy powder. The powder X-ray diffraction patterns of the nanoporous materials before and after compaction at 8000 lb are shown in Figure 3.

Although the XRD patterns indicate that all of the nanoporous materials exhibit a decrease in structural ordering upon compression at 8000 lb, the degree of this change differs considerably from one material to another. The methylene-bridged PMO and the nanoporous silica both exhibit a substantial decrease in the intensity and broadening of their (100) reflections. The phenylene-bridged PMO shows a less-pronounced decrease in intensity but a noticeable increase in the full width at half-maximum. The ethylene-bridged PMO (Figure 3b) exhibits the

TABLE 2: Physicochemical Properties of Extracted Nanoporous Organosilicas before and after Mechanical Treatments

sample	D^a (Å)	BET surface area (m^2/g)	total pore volume (cm^3/g)	pore size[b] (Å)
methylene PMO	74	870	0.90	50
methylene PMO (8 K)		470	0.20	26
ethylene PMO	63	1080	1.10	43
ethylene PMO (4 K)	63	1060	1.10	44
ethylene PMO (8 K)	63	1010	0.90	40
phenylene PMO	57	901	0.60	33
phenylene PMO (8 K)	57	650	0.30	26
nanoporous silica	59	1010	1.30	44
nanoporous silica (2 K)	55	780	0.70	39
nanoporous silica (4 K)	55	570	0.30	26
nanoporous silica (8 K)		390	0.10	23

[a] $d(100)$ spacing of the extracted products (±2 Å). [b] Calculated from adsorption branch.

highest mechanical stability. The best indication of decreased structural ordering in this material is the rather poor resolution of the (200) and (110) reflections following compression. It should be noted that these secondary reflections are no longer present in the silica sample following mechanical treatment. Because our results indicated that the ethylene-bridged PMO had the highest mechanical stability, while a near-complete collapse in pore structure was exhibited by the nanoporous silica, these two materials were investigated further by pressing at both 4000 lb (134 MPa) and 2000 lb (67 MPa) for 30 min. The physicochemical properties of the organosilicas before and after compaction are given in Table 2.

Nitrogen gas sorption isotherms and Bopp−Jancso−Heinzinger (BJH) pore size distributions (insets) shown in Figure 4 further illustrate the effects of mechanical compression on the nanoporous materials. The methylene-bridged PMO (Figure 4a) exhibits an 80% decrease in total pore volume, a decrease in the pore size distribution maximum from 50 to 26 Å, and a 50% decrease in surface area. The ethylene-bridged PMO shows better mechanical stability but still exhibits a decrease in total pore volume of ~18% upon compression at 8000 lb for 30 min. It is interesting to note that the nitrogen adsorption isotherms of the ethylene- and phenylene-bridged PMOs (Figure 4b,c) do not change significantly in the microporous region from those of the untreated samples. In contrast, the step in the mesoporous region decreases noticeably. This seems to indicate that the changes in the microstructure in these materials is due to a collapse of mesopores, while the micropores contained primarily in the pore walls remain unchanged. This is in stark contrast to what is shown by the methylene-bridged PMO, which exhibits a large decrease in micropore volume upon pressing. The pore size distributions of the ethylene-bridged PMO show little change upon compression.

The nitrogen gas adsorption isotherms and pore size distributions of the nanoporous silica subjected to compression at various pressures are shown in Figure 4d. In agreement with our XRD data, the pure silica sample is less-stable under high-pressure conditions than any of the three PMOs characterized in this study. At 8000 lb, the silica exhibits a 90% decrease in total pore volume, a decrease in pore size from 44 to 23 Å, and a decrease in BET surface area from 1010 to 390 m^2/g (Table 2).

To determine whether the surfactant templates could improve the mechanical stability of the nanostructured materials, the as-synthesized composites were also pressed at 8000 lb for 30 min. The powder X-ray diffraction patterns are shown in Figure 5. It is interesting to note that the mechanical stabilities of the methylene-bridged PMO and the silica, the two materials that exhibited the lowest mechanical stability in their porous (template-free) state, are improved significantly if the templates are present. The X-ray diffraction patterns (Figures 5a,d) show

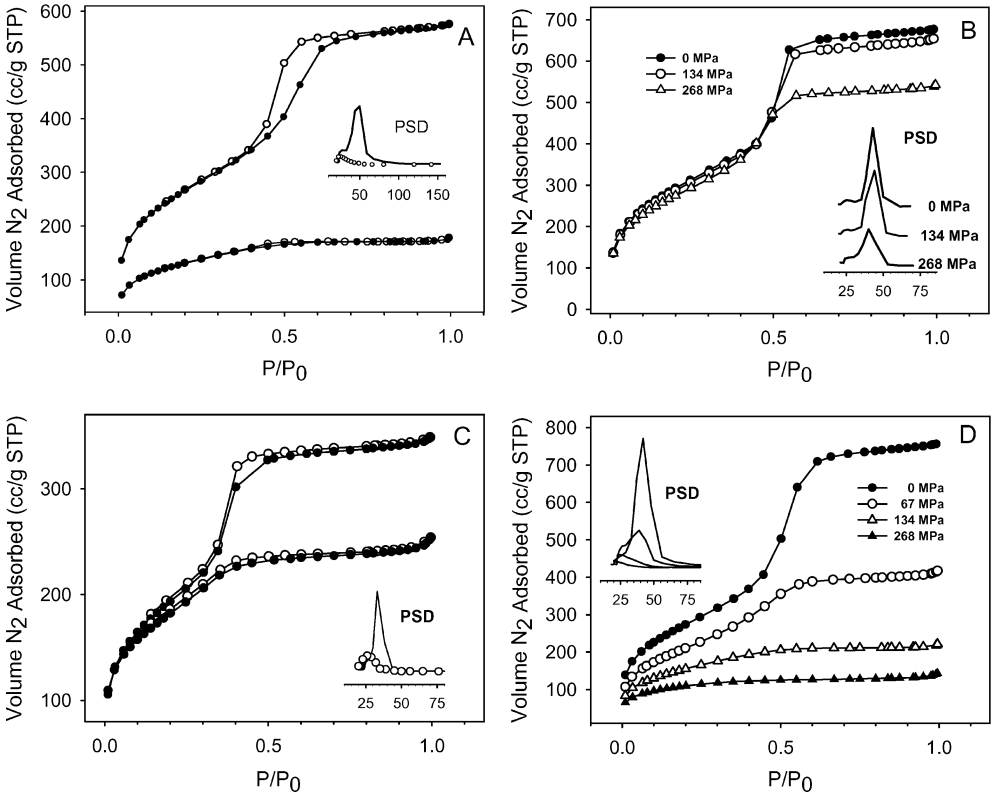

Figure 4. Nitrogen gas adsorption/desorption isotherms and pore size distributions (insets, PSD) of template-extracted (A) methylene, (B) ethylene, (C) phenylene, and (D) silica nanoporous materials before and after pressure treatment.

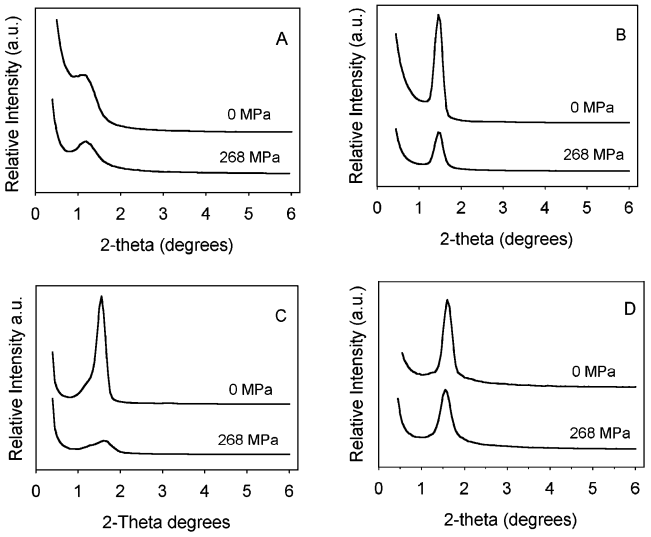

Figure 5. Powder X-ray diffraction patterns of the as-synthesized (A) methylene, (B) ethylene, (C) phenylene, and (D) silica composite materials before and after pressure treatment at 268 MPa for 30 min.

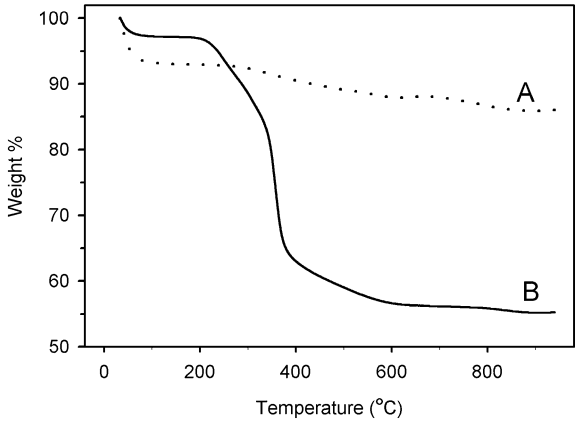

Figure 6. Thermogravimetric weight loss curves of (A) extracted and (B) as-synthesized methylene-bridged PMO.

little difference after high-pressure treatment. This stabilizing effect of surfactant templates has been reported before.[4,28] Surprisingly, the (100) reflection of the as-synthesized phenylene-bridged PMO exhibits a significant decrease in intensity.

Thermogravimetric analyses were performed (20−1000 °C) on all of the as-synthesized and extracted nanostructured materials prior to mechanical treatment. The amount of residual water and ethanol can be easily estimated because they come off at temperatures below 150 °C, before most matrix decomposition occurs. The thermogravimetric weight loss curves of the as-synthesized and extracted methylene-bridged PMO shown in Figure 6 are typical. While the total weight loss for the as-synthesized composite (Figure 6B) is much larger than that of the extracted material (Figure 6A), the weight loss due to residual water and ethanol (∼3%) is less than half that of the porous sample (∼7%). The larger total weight loss of the as-synthesized composite can be attributed to the decomposition of the surfactant (∼34%), which is not present in the extracted material. The presence of residual ethanol in all of the extracted material was evident in the ^{13}C MAS NMR spectra at resonances $\delta \approx 18$ (methyl) and 58 (methylene) ppm (Figure 2). The increase in the amount of adsorbed water and ethanol following extraction is likely due to the significant increase in surface area and overall decrease in hydrophobicity resulting from template removal. The percent weight loss due to residual water and ethanol and the total percent weight loss for the nanoporous materials are listed in Table 3.

TABLE 3: Thermogravimetric Properties of Extracted and As-Synthesized Composite Nanoporous Materials

sample	H_2O−EtOH weight loss[a] (%)	total weight loss[b] (%)	H_2O−EtOH/total ratio
methylene PMO	7.0	14.0	0.50
methylene PMO (as)	3.0	44.0	0.07
ethylene PMO	4.0	16.5	0.23
ethylene PMO (as)	2.0	49.0	0.04
phenylene PMO	12.0	34.0	0.35
phenylene PMO (as)	12.0	38.0	0.31
nanoporous silica	13.0	22.0	0.59
nanoporous silica (as)	2.0	57.0	0.03

[a] Percentage weight loss up to 150 °C. [b] Percentage weight loss up to 950 °C.

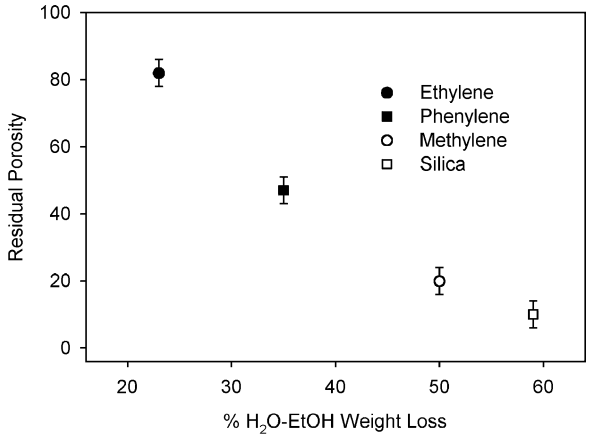

Figure 7. Percentage of water−ethanol weight loss versus residual porosity for nanoporous materials following pressure treatment at 268 MPa.

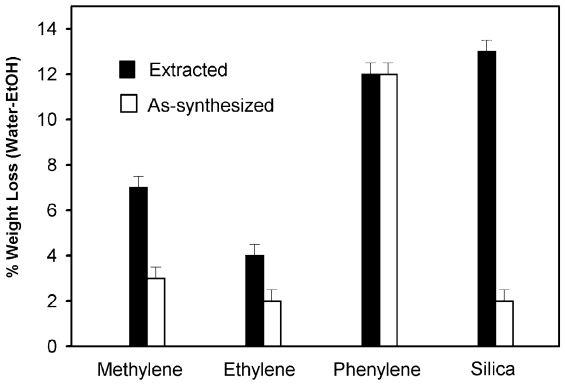

Figure 8. Thermogravimetric weight loss curves of as-synthesized and extracted methylene, ethylene, phenylene, and silica composite materials.

The collapse of ordered nanoporous silicas during compression has been explained in terms of a mechanochemical hydrolysis of siloxane groups.[29] A comparison of the residual water and ethanol present in the nanoporous materials with their mechanical stabilities is therefore in order. Thermogravimetric analyses of our organosilicas show that those containing larger organic bridging groups such as ethylene and phenylene lose more weight due to matrix decomposition. However, the relatively smaller bridging group methylene and silica materials show a higher percent weight loss due to water−ethanol indicating that these materials contain more water and ethanol within the pores. Therefore, the ratio of the weight loss due to

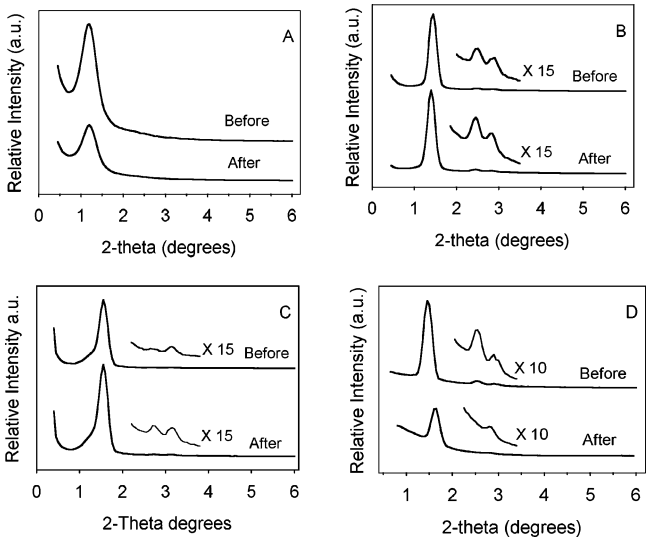

Figure 9. Powder X-ray diffraction patterns of template-extracted (A) methylene, (B) ethylene, (C) phenylene, and (D) silica nanoporous materials before and after hydrothermal treatment.

residual water and ethanol to the total weight loss can represent the hydrophilic character of these materials. The hydrophilicity increased in the order ethylene < phenylene < methylene < silica. The increase in the carbon chain length and the size of the nonpolar organic molecule can be contributing factors for the decreased hydrophilicity in ethylene- and phenylene-bridged organosilicates.[30] Therefore the inclusion of these bridging structures will impart hydrophobic/hydrophilic characteristics to the organosilicates. The total pore volumes (from nitrogen sorption) measured before and after compression at 8 K have been used to calculate the residual porosity, an accurate representation of mechanical stability. The water−ethanol weight loss ratios are plotted against the residual porosity in Figure 7. The more hydrophobic materials exhibit the best mechanical stability. This trend supports the hypothesis that the mechanism of structural collapse in these materials involves mechanochemical hydrolysis. A comparison of the thermogravimetric data of the as-synthesized composites with those of the extracted samples (Figure 8) illustrates this trend once again. In general, the as-synthesized composites are more hydrophobic. This explains their enhanced mechanical stability over the extracted samples, as indicated by XRD data (Figures 3 and 5). The surprising instability of the phenylene as-synthesized composite (Figure 5c) can now be explained in terms of its relatively high water content measured by TGA. The reasons for the relatively high hydrophilic character of the phenylene PMO are not fully understood at this time.

Hydrothermal Stability. Powder X-ray diffraction and nitrogen sorption measurements were performed on the aged nanoporous materials before and after hydrothermal treatments. The X-ray diffraction results shown in Figure 9 indicate no structural degradation in any of the PMOs after hydrothermal treatment. In fact, the ethylene- and phenylene-bridged PMOs exhibit a moderate hydrothermal restructuring that improves the order of their microstructures. The ethylene-bridged PMO (Figure 9b) shows slight increases in the intensities of its (100), (110), and (200) reflections. The phenylene-bridged PMO (Figure 9c) shows an increase in its (100) and (200) peaks and significant enhancement of the (110) reflection at $2\theta = 2.70$, indicating hexagonal ordering (*P6mm* space group). The methylene-bridged PMO (Figure 9a) shows little change in its wormhole microstructure after treatment. Unlike our PMOs, diffraction on nanoporous silica (Figure 9d) shows a decrease in the intensity of both the (100) and (110) reflections and the disappearance of the (200) peak, indicating reduced structural ordering after hydrothermal treatment. The (100) and (110) reflections are also shifted to higher values of 2θ.

Nitrogen gas sorption analyses were performed on all of the extracted nanoporous samples before and after hydrothermal treatments. All exhibit type IV isotherms (Figure 10) with a large step in the mesoporous range and sharp BJH pore size distributions (insets). The physicochemical properties of the nanoporous materials are listed in Table 4. In agreement with the X-ray data, only the nanoporous silica shows any significant damage. The hydrothermally treated sample exhibits an increase in pore size, a corresponding decrease (∼35%) in surface area,

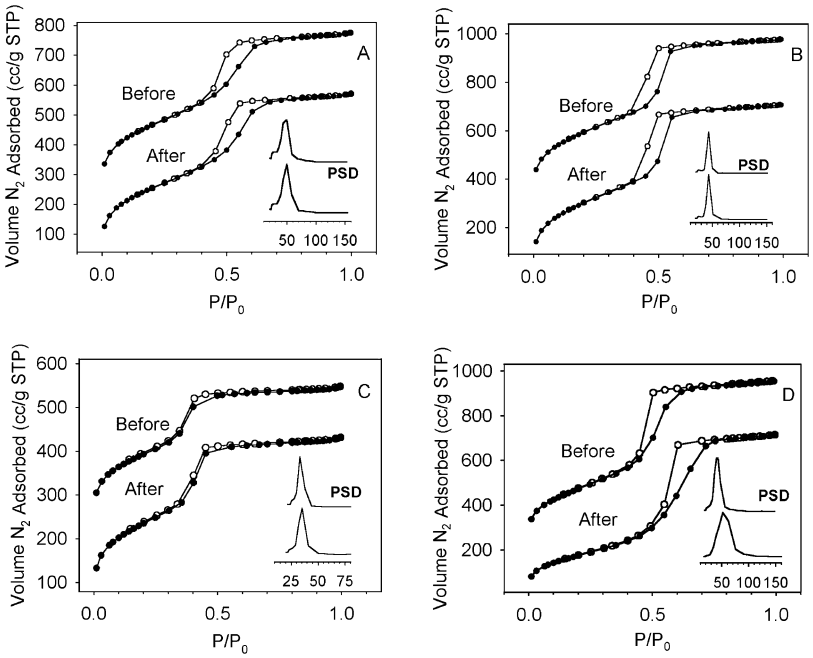

Figure 10. Nitrogen gas adsorption/desorption isotherms and pore size distributions (insets, PSD) of template-extracted (A) methylene, (B) ethylene, (C) phenylene, and (D) silica nanoporous materials before and after hydrothermal treatment.

TABLE 4: Structural Properties of Extracted Nanoporous Organosilicas before and after Hydrothermal Treatment

sample	D^a (Å)	BET surface area (m^2/g)	total pore volume (cm^3/g)	pore size[b] (Å)	wall thickness[c] (Å)
methylene PMO (aged)	74	870	0.90	50	35
methylene PMO (hydro)	74	930	1.00	50	35
ethylene PMO (aged)	63	1080	1.10	43	29
ethylene PMO (hydro)	63	1120	1.20	43	30
phenylene PMO (aged)	57	900	0.60	33	33
phenylene PMO (hydro)	57	850	0.70	35	31
nanoporous silica (aged)	59	1010	1.30	44	24
nanoporous silica (hydro)	53	660	1.10	52	9

[a] $d(100)$ spacing of the extracted products (±2 Å). [b] Calculated from adsorption branch. [c] Estimated from a_0-pore size, where $a_0 = (2\sqrt{3}/3)d(100)$.

and a significant decrease in wall thickness from 24 to 9 Å. Unlike most template-free silicas, which are destroyed after 18 h of boiling, the high hydrothermal stability observed in our nanoporous materials is most likely due to the thicker pore (24−35 Å) walls obtained through synthesis with alkylethylene oxide templates in acidic media. A similar result has been reported recently for an ethane-bridged PMO synthesized using Pluronic 123 as the structure director.[31]

Conclusions

We have reported the effects of aging, mechanical, and hydrothermal treatments on the microstructures of periodic mesoporous organosilicas (PMOs). Methylene-, ethylene-, and phenylene-bridged PMOs and ordered mesoporous silica were synthesized by acid-catalyzed hydrolysis and condensation of bis(triethoxysilyl) precursors around supramolecular polyoxyethylene(10) stearyl ether (Brij 76) templates. The PMOs were then generated by extraction of the templates. As-synthesized composites containing surfactant templates have also been characterized and compared to the PMOs derived from them. None of the nanoporous materials in this study exhibited any significant changes in microstructure following aging for 10 months under ambient conditions. Results obtained from XRD, nitrogen sorption, and thermogravimetric analyses support the concept of mechanochemical silicate hydrolysis as the driving force behind microstructural collapse in these nanoporous materials. All three PMOs in this study exhibited better mechanical and hydrothermal stabilities than periodic mesoporous silica. Future experiments will include an investigation of the mechanical stabilities of PMOs after hydrothermal treatment.

Acknowledgment. Dr. Shalini Jayasundera and Dr. Chris W. Thomas are NRC/NRL Research Fellows. The authors thank Dr. Mazyar Zeinali for many helpful discussions. This project was funded by the Office of Naval Research through a Naval Research Laboratory Accelerated Research Initative.

References and Notes

(1) Kresge, C. T.; Leonowicz, M. E.; Roth, W. J.; Vartuli, J. C.; Beck, J. S. *Nature* **1992**, *359*, 710.

(2) Beck, J. S.; Vartuli, J. C.; Roth, W. J.; Leonowicz, M. E.; Kresge, C. T.; Schmitt, K. D.; Chu, C. T.; Olson, D. H.; Sheppard, E. W.; McCullen, S. B.; Higgins, J. B.; Schlenker, J. L. *J. Am. Chem. Soc*. **1992**, *114*, 10834.

(3) Huo, Q.; Margolese, D. I.; Stucky, G. D. *Chem. Mater*. **1996**, *8*, 1147.

(4) Zhao, D.; Huo, Q.; Feng, J.; Chmelka, B. F.; Stucky, G. D. *J. Am. Chem. Soc*. **1998**, *120*, 6024.

(5) Kim, J. M.; Ryoo, R. *Bull. Korean Chem. Soc*. **1996**, *17*, 66.

(6) Ryoo, R.; Jun, S. *J. Phys. Chem. B* **1997**, *101*, 317.

(7) Kim, J. M.; Jun, S.; Ryoo, R. *J. Phys. Chem. B* **1999**, *103*, 6200.

(8) Mokaya, R. *J. Phys. Chem. B* **1999**, *103*, 10204.

(9) Cassiers, K.; Linssen, T.; Mathieu, M.; Benjelloun, M.; Schrijnemakers, K.; Van Der Voort, P.; Cool, P.; Vansant, E. F. *Chem. Mater*. **2002**, *14*, 2317.

(10) Shen, S. C.; Kawi, S. *J. Phys. Chem. B* **1999**, *103*, 8870.

(11) Mokaya, R. *J. Phys. Chem. B* **2000**, *104*, 8279.

(12) Broyer, M.; Valange, S.; Bellat, J. P.; Bertrand, O.; Weber, G.; Gabelica, Z. *Langmuir* **2002**, *18*, 5083.

(13) Koyano, K. A.; Tatsumi, T.; Tanaka, Y.; Nakata, S. *J. Phys. Chem. B* **1997**, *101*, 9436.

(14) Hartmann, M.; Vinu, A. *Langmuir* **2002**, *18*, 8010.

(15) Wu, J.; Liu, X.; Tolbert, S. H. *J. Phys. Chem. B* **2000**, *104*, 11837.

(16) Feng, X.; Fryxell, G. E.; Wang, L. Q.; Kim, A. Y.; Liu, J.; Kemner, K. M. *Science* **1997**, *276*, 923.

(17) Liu, J.; Feng, X.; Fryxell, G. E.; Wang, L. Q.; Kim, A. Y.; Gong, M. *Adv. Mater*. **1998**, *10*, 161.

(18) Dai, S.; Shin, Y.; Ju, Y.; Burleigh, M. C.; Lin, J. S.; Barnes, C. E.; Xue, Z. *Adv. Mater*. **1999**, *11*, 1226.

(19) Burkett, S. L.; Sims, S. D.; Mann, S. *Chem. Commun*. **1996**, 1367.

(20) Macquarrie, D. J. *Chem. Commun*. **1996**, 1961.

(21) Fowler, C. E.; Burkett, S. L.; Mann, S. *Chem. Commun*. **1997**, 1769.

(22) Yoshina-Ishii, C.; Asefa, T.; Coombs, N.; MacLachlan, M. J.; Ozin, G. A. *Chem. Commun*. **1999**, 2539.

(23) Inagaki, S.; Guan, S.; Fukushima, Y.; Ohsuna, T.; Terasaki, O. *J. Am. Chem. Soc.* **1999**, *121*, 9611.

(24) Melde, B. J.; Holland, B. T.; Blanford, C. F.; Stein, A. *Chem. Mater*. **1999**, *11*, 3302.

(25) Burleigh, M. C.; Markowitz, M. A.; Spector, M. S.; Gaber, B. P. *J. Phys. Chem. B* **2002**, *106*, 9712.

(26) Burleigh, M. C.; Jayasundera, S.; Thomas, C. W.; Spector, M. S.; Markowitz, M. A.; Gaber, B. P. *Colloid Polym. Sci*., in press.

(27) Bennet, A. E.: Rienstra, C. M.: Auger, M.: Lakshmi, K. V.: Griffin, R. G. *J Chem Phys.* **1995**, *103*, 6951.

(28) Beck, J. S.; Vartuli, J. C.; Roth, W. J.; Leonowicz, M. E.; Kresge, C. T.; Schmitt, K. D.; Chu, C. T.-W.; Olson, D. H.; Sheppard, E. W.; McCullen, S. B.; Higgins, J. B.; Schlenker, J. L. *J. Am. Chem. Soc*. **1992**, *114*, 10834.

(29) Tatsumi, T.; Koyano, K. A.; Tanaka, Y.; Nakata, S. *J. Porous Mater*. **1999**, *6*, 13.

(30) Schwarzenbach, R. P.; Gschwend, P. M.; Imboden, D. M. *Environmental Organic Chemistry*; John Wiley & Sons: New York, 1993.

(31) Guo, W. P.; Park, J. Y.; Oh, M. O.; Jeong, H. W.; Cho, W. J.; Kim, I.; Ha, C. S. *Chem. Mater*. **2003**, *15*, 2295.